# Nanoscale

Accepted Manuscript


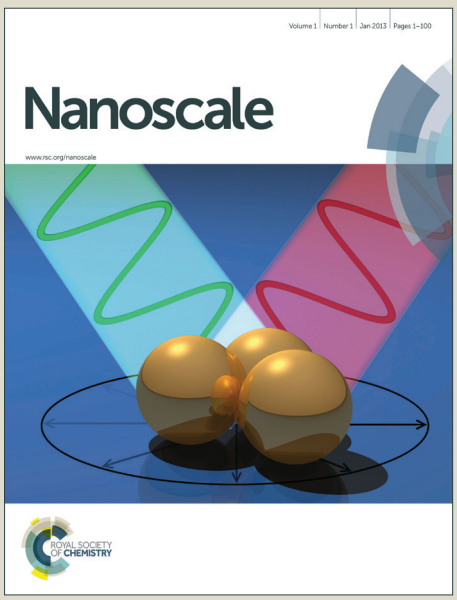





ROYAL SOCIETY OF CHEMISTRY

www.rsc.org/nanoscale

# Flexible nitrogen-doped graphene/carbon nanotube/$Co_3O_4$ paper and its oxygen reduction activity †

Shan-Shan Li,[a] Huai-Ping Cong,*[a,b] Ping Wang[a] and Shu-Hong Yu*[a]



[a] Division of Nanomaterials & Chemistry, Hefei National Laboratory for Physical Sciences at Microscale, Department of Chemistry, University of Science and Technology of China, Hefei 230026, P. R. China.
E-mail: shyu@ustc.edu.cn, hpcong@hfut.edu.cn Fax: 0086 551 63603040

[b] Anhui Key Laboratory of Controllable Chemical Reaction and Material Chemical Engineering, School of Chemical Engineering, Hefei University of Technology, Hefei, Anhui, 230009, P. R. China. E-mail: hpcong@hfut.edu.cn

† Electronic supplementary information (ESI) available. XRD patterns, elemental mapping images, DSC-TGA curves and XPS spectrum of NG/CNT/$Co_3O_4$ paper; SEM images and XPS spectra of NG/$Co_3O_4$ paper; RDE curves and corresponding K-L plots of different catalysts.

**Table of contents entry**

A new kind of flexible nitrogen-doped graphene/carbon nanotube/$Co_3O_4$ paper has been fabricated in large scale by a facile but effective strategy in combinations of the self-assembly process and hydrothermal treatment, behaving a promising candidate as oxygen reduction electrocatalyst.

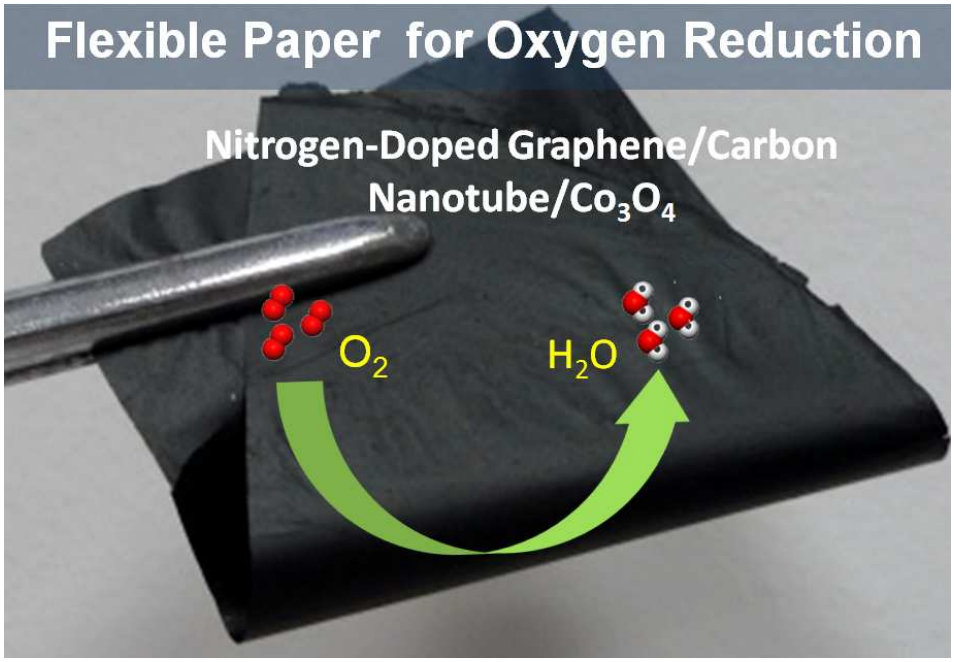


**Keywords:** nitrogen-doped graphene, carbon nanotube, $Co_3O_4$, electrocatalyst, oxygen reduction, methanol-tolerant.

**Abstract:** On demanding of the high-efficient, costless and scalable synthesis of oxygen reduction reaction (ORR) catalyst for the practical application in fuel cell, we demonstrate a facile strategy to fabricate the flexible nitrogen-doped graphene/carbon nanotube/$Co_3O_4$ (NG/CNT/$Co_3O_4$) paper catalyst. In the hydrothermal process, *in-situ* formation of $Co_3O_4$ nanoparticles, reduction of GO and doping of nitrogen species occur simultaneously in the assembled paper in ammonia solution. Owing to the synergistic effects of three active components and the spacing effect of CNTs and $Co_3O_4$ nanoparticles on avoiding the re-aggregation of assembled graphene nanosheets, the free-standing NG/CNT/$Co_3O_4$ paper shows the enhanced ORR catalytic performance with the stable durability and strong methanol-tolerant capability, behaving the promising potentials as the ORR electrocatalyst in the practical application.

## Introduction

Developing the effective electrocatalyst for cathodic oxygen reduction reaction (ORR) is one of the most crucial factors in the performance of a fuel cell.[1] Platinum-based materials have been widely researched as the most active catalysts for ORR, but their high cost, sensitivity to methanol and CO, weak durability hinder the large-scale application of fuel cells.[2] To overcome this obstacle, non-precious metal chalcogenides,[3] oxides,[4] nitrides[5] and organometallic complexes[6,7] have been developed as platinum-based catalyst alternatives. However, the activity and stability of these materials for ORR are still far from the requirements for practical applications of fuel cell.

Recently, nitrogen-doped carbon materials, especially nitrogen-doped graphene (NG), have been extensively investigated as ORR electrocatalysts.[8,9] The incorporation of N element into graphene

can improve their electrocatalytic performance owing to the formed delocalized conjugated system between the lone electron pairs of N atoms and the $sp^2$-hybridized carbon frameworks.[10] Parts of these NG show comparable ORR activities to commercial Pt/C catalyst, with better long-term stability, stronger tolerance to crossover and poison effect.[11] Up to now, the main synthesis methods for NG include chemical vapor deposition,[12] arc-discharge,[13] plasma treatment,[14] high temperature treatment[10, 15] and so on. However, rigorous conditions, special instruments and toxicity of the nitrogen precursors ($NH_3$, pyridine or pyrrole) at high temperature limit the NG in the practical applications.[9]

Apart from intrinsic catalytic reactivity, NG is also suitable to act as support for loading transition metal oxide[16-20]/chalcogenide nanocrystals[21,22] owing to their excellent electrical property, high surface area, good chemical stability, and strong adhesion to catalyst particles.[19] These strongly-coupled hybrids exhibit much higher electrocatalytic activity than that of either non-precious metals or NG alone.[23] For example, Dai and coworkers[16] designed and synthesized the NG/$Co_3O_4$ nanocomposites by a two-step solution-phase method, which showed high electrocatalytic activity in alkaline solutions and was superior to commercial Pt/C in terms of stability.

On the other hand, composite materials composed of graphene and carbon nanotube (CNT) have been extensively studied in the fields of transparent conductors,[24] photocatalysis,[25] lithium-ion batteries,[26] supercapacitors,[27] and fuel cells.[28] CNT existed between the graphene nanosheets not only prevent graphene from restacking and increase the basal spacing, but also bridge the defects for electron transfer and improve the electrical conductivity.[29] Thus, these graphene/CNT composite materials display significant enhancement of the electrochemical performance compared with the

single graphene. Recently, we have synthesized the NG-CNT nanocomposites with the synergistic enhancement of electrochemical ORR activities by a mild hydrothermal process at low temperature.[28] However, up to now, most of the reported work on preparing ORR electrode material has been focused on the dispersion of active powder and binder (*eg.* Nafion) with time-consuming ultrasonic treatment. Compared with the powdery materials, the freestanding graphene-based paper by the easily scaled-up synthesis method as the electrode material avoids the conventional tedious processing procedure of electrode making, and thus, in this regard, shows promising potentials in the practical applications.[30]

Herein, a novel kind of flexible nitrogen-doped graphene/carbon nanotube/$Co_3O_4$ (NG/CNT/$Co_3O_4$) paper has been synthesized in large scale by combining a convenient self-assembly strategy with the following facile hydrothermal treatment. Interestingly, *in-situ* formation of $Co_3O_4$ nanoparticles, reduction of GO and doping of nitrogen species occurred simultaneously in the assembled paper with the hydrothermal process in ammonia solution. Owing to the synergistic effects of three components, the freestanding NG/CNT/$Co_3O_4$ paper directly adhered to the glass carbon (GC) disk as the working electrode showed enhanced ORR electrocatalytic performances with the positive onset potential and high current density. Furthermore, as-prepared NG/CNT/$Co_3O_4$ paper exhibited much better cycling stability and stronger resistance to methanol crossover effects than the commercial Pt/C catalyst, making it a promising candidate as the ORR electrode material.

**Experimental section**

**Preparation of NG/CNT/$Co_3O_4$ paper.** Above all, graphene oxide (GO)[31] and oxidized carbon nanotube (CNT) [28] suspensions were prepared, respectively, according to previously-reported work.

In the typical synthesis step of $Co^{2+}$-GO/CNT paper, 10 mL of 2 mg/mL GO and 1 mL of 2 mg/mL CNT aqueous suspensions were mixed together under magnetic stirring in a beaker. Then, 0.2 mL of 1 M $Co(NO_3)_2$ aqueous solution was added to above suspension. The uniform mixture was coated on a Teflon substrate followed by placing in an oven at 80 $^oC$ for 2 h. After peeling off the $Co^{2+}$-GO/CNT paper from the Teflon substrate, the above paper was immersed into the 3.3 vol.% ammonia solution and transferred into an autoclave. After the hydrothermal treatment at 180 ℃ for 2 h, NG/CNT/$Co_3O_4$ paper was obtained, finally. The controlled samples of NG, NG/CNT and NG/$Co_3O_4$ papers were fabricated by the similar procedures of NG/CNT/$Co_3O_4$. Physically-mixed NG/CNT/$Co_3O_4$ was fabricated by the similar procedures of NG/CNT/$Co_3O_4$ except that $Co(NO_3)_2$ was replaced by $Co_3O_4$ nanoparticles prepared in advance.

**Characterization**. SEM images were carried out on a Zeiss Supra 40 field emission scanning electron microanalyzer at an acceleration voltage of 5 kV. TEM images were recorded on Hitachi H-7650 with an acceleration voltage of 200 KV. HRTEM, EDS, scanning TEM and element mapping analysis were taken on a JEOL-2010F transmission electron microscope equipped with Oxford Inca. XRD patterns were carried out on a PW1710 instrument with Cu $K_\alpha$ radiation ($\lambda$ = 1.5406 Å). XPS measurements were performed on an ESCALab MKII X-ray photoelectron spectrometer using Mg Ka radiation exciting source. DSC-TGA measurements were carried out on a thermal analyzer (SDT Q600, TA instruments, USA) with a heat rate of 10 K $min^{-1}$ in air.

**ORR activities.** The Electrochemical measurements were performed by a conventional three-electrode cell using IM6e electrochemical workstation (Zahner-Electrik, Germany) at room temperature. A glass carbon (GC) electrode loading with the electrocatalyst, Ag/AgCl electrode and platinum plate were used as the working electrode, reference electrode and counter electrode,

respectively. For the preparation of working electrode, free-standing paper with the size of 5 x 5 mm was directly adhered onto the GC electrode with the diameter of 5 mm using 5 μL Nafion solution (0.5 wt%) as binder and dried at ambient condition. CVs were carried out in a 0.1 M KOH solution at a scan rate of 100 mV $s^{-1}$. RDE measurements were conducted in $O_2$-saturated 0.1 M KOH solution at the scan rate of 10 mV $s^{-1}$ with varying rotating speed from 400 to 2025 rpm. The kinetic parameters were analyzed on the basis of the Koutecky-Levich (K-L) equations.[2]

**Results and discussion**

**Fabrication of flexible NG/CNT/$Co_3O_4$ paper**

**Fig. 1**a schematically illustrated the formation mechanism of NG/CNT/$Co_3O_4$ composite paper. Firstly, well-dispersed CNT aqueous suspension was obtained by the oxidation of multi-walled carbon nanotubes according to the preparation procedures of graphene oxide (GO) dispersion by the modified Hummers method.[31] Then, CNT and $Co(NO_3)_2$ aqueous solutions were gradually added to the GO dispersion under magnetic stirring in sequence. In this way, positively-charged $Co^{2+}$ was deposited on the surfaces of negatively-charged GO and CNT due to the electrostatic attraction between oxygen-containing groups of GO and CNT and metal ions. By coating a thin layer of the above mixture on a Teflon substrate and then placing in an oven at 80 $^oC$ for 2 h, a typical freestanding $Co^{2+}$-decorated GO/CNT paper ($Co^{2+}$-GO/CNT) with a multilayer structure was prepared via the evaporation-induced assembly based on π-π stacking interaction of GO sheets (Fig. 1a). Moreover, the spacing effect of CNT and $Co^{2+}$ facilitated the formation of ordered assembly structure in the paper, which effectively avoided the re-aggregation of GO sheets. In this step, no cobalt oxide nanoparticle was formed in the assembly process of GO/CNT paper, as concluded from no diffraction peak in the XRD pattern (ESI, Fig. S1a†). After peeling off from the substrate, the

$Co^{2+}$-GO/CNT composite paper was hydrothermally treated in the ammonia solution at 180 °C. With prolonging the hydrothermal time, a piece of flexible paper composed of NG sheets, CNTs and $Co_3O_4$ nanoparticles was obtained as shown from the time-dependent XRD patterns of NG/CNT/$Co_3O_4$ papers (ESI, Fig. S1†).

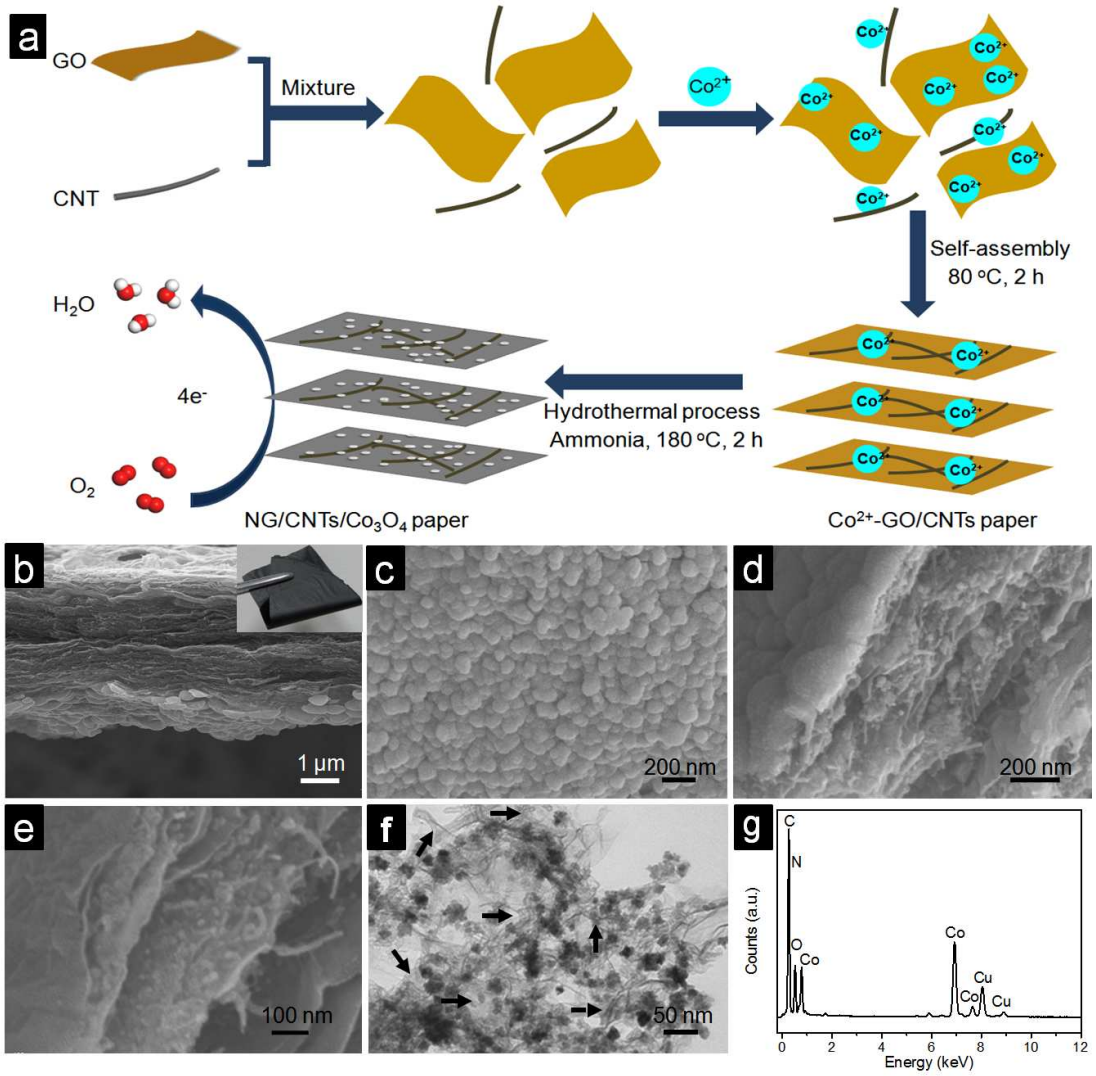


**Fig. 1** (a) Schematic illustration of the preparation of the NG/CNT/$Co_3O_4$ composite paper. (b) SEM image of the cross-section of NG/CNT/$Co_3O_4$ paper. The inset photograph showing a flexible paper. (c) SEM image of the outer surface of NG/CNT/$Co_3O_4$ paper. (d and e) Low and high magnified SEM images of the cross-section of NG/CNT/$Co_3O_4$ paper. (f) TEM image of the NG/CNT/$Co_3O_4$ paper with long-time ultrasonication. The black arrows showing the loaded CNTs. (g) EDX image of NG/CNT/$Co_3O_4$ paper in Figure (f).

**Characterization of flexible NG/CNT/$Co_3O_4$ paper**

Fig. 1b-1f showed representative SEM and TEM images of the NG/CNT/$Co_3O_4$ paper. The flexible paper (ESI, Fig. S2†) with the ordered multilayer structure was measured to be *ca.* 4 μm in thickness according to the cross-section SEM image (Fig. 1b). Interestingly, a monolayer of $Co_3O_4$ nanoparticles with the size of about 100 nm was formed on the surface of the composite paper as shown from the magnified SEM image (Fig. 1c). Furthermore, the magnified SEM images of the cross-section of the paper revealed abundant of CNTs and $Co_3O_4$ nanoparticles existing between the graphene nanosheets (Fig. 1d and 1e). Moreover, CNTs were well-stacked in the horizontal direction owing to the restriction of full length extension of the flexible CNTs in the space within the graphene layers and the two-dimensional structure of the graphene sheets. The graphene sheets acted as strong holders with large area to support the organization of the CNTs.[32] TEM image of the NG/CNT/$Co_3O_4$ paper with the long-time ultrasonic treatment further indicated the uniform decorations of $Co_3O_4$ nanoparticles with the size of about 25 nm and CNTs marked by black arrows on the graphene nanosheets (Fig. 1f). Energy dispersive X-ray (EDX) image revealed the presence of C, N, O and Co elements in the composite paper (Fig. 1g).

The XRD pattern of NG/CNT/$Co_3O_4$ paper (**Fig. 2**a) showed the broad diffraction peak with low intensity at 2θ of about 25°, indexed into the (002) plane of the disorderedly stacked graphene sheets.[33] All of the other diffraction peaks were ascribed to the $Co_3O_4$ phase with a face-centered cubic structure (JCPDS No. 42-1467). HRTEM image of the $Co_3O_4$ nanoparticle displayed clear lattice fringes with the distance of approximate 0.46 nm, corresponding to the lattice spacing of the $Co_3O_4$ (111) plane (ESI, Fig. S3a†), confirmed the formation of $Co_3O_4$ nanocrystals in the composite paper. DSC-TGA curves revealed that there were 20.9 wt % of $Co_3O_4$ nanoparticles in the paper (ESI, Fig. S4†). The survey XPS spectrum showed the existence of C, O and Co elements

in the initial $Co^{2+}$-GO/CNT paper (Fig. 2b). With the hydrothermal treatment of the initial $Co^{2+}$-GO/CNT paper in ammonia solution, the obtained NG/CNT/$Co_3O_4$ paper was composed of C, N, O and Co elements, as shown from the survey XPS spectrum (Fig. 2b). The C1s core-leveled XPS spectra showed the changes of the contents of different types of carbon species before and after hydrothermal treatment (Fig. 2c). In the initial $Co^{2+}$-GO/CNT paper, there were 65 % of C=C at 284.2 eV and 35 % of C-O/C=O at the higher binding energies. However, in NG/CNT/$Co_3O_4$ paper, the significantly-weakened bands at high binding energies indicated the decreased content of oxygen-containing carbon groups, due to the effective reduction of GO by removing most of the oxygen-containing groups of GO with hydrothermal process.[34] The Co2p core-leveled XPS spectrum of NG/CNT/$Co_3O_4$ paper (ESI, Fig. S5†) showed two peaks at 781 and 797 eV, assigned to $Co2p_{3/2}$ and $Co2p_{1/2}$ for $Co_3O_4$, respectively.[34]

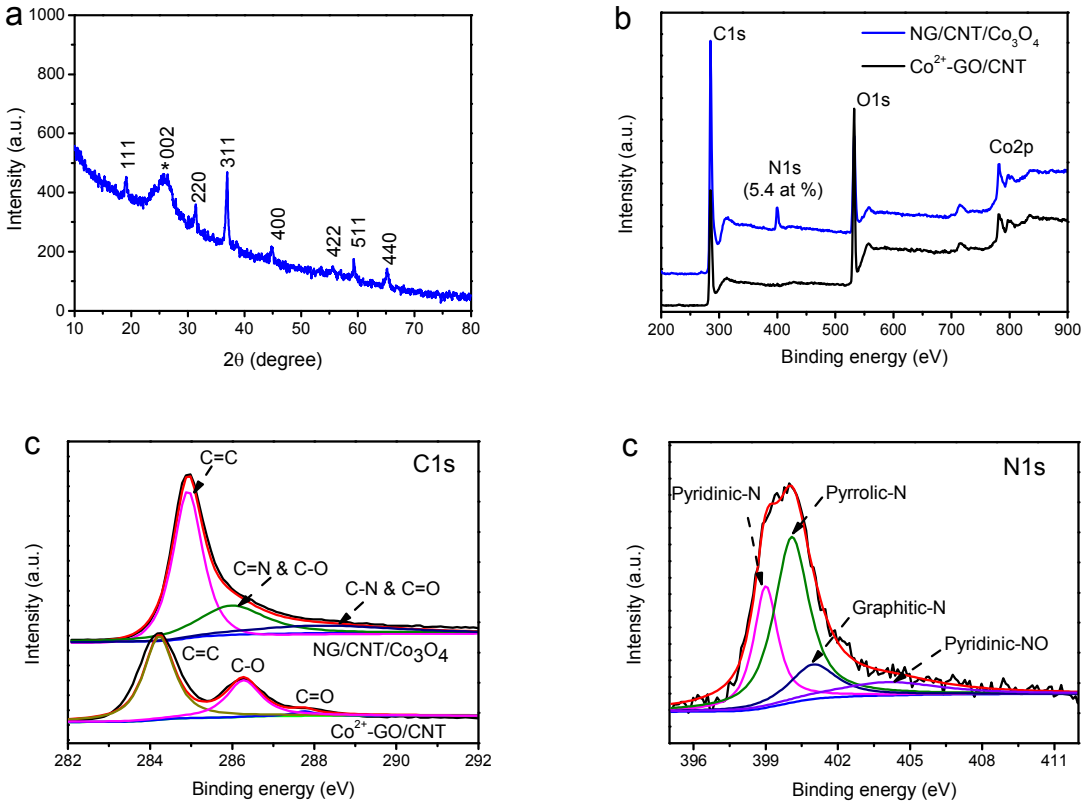

**Fig. 2** (a) XRD pattern of NG/CNT/$Co_3O_4$ paper. (b) Survey XPS spectra of NG/CNT/$Co_3O_4$ and $CO^{2+}$-GO/CNT papers. (c) C1s core-leveled XPS spectra of NG/CNT/$Co_3O_4$ and $CO^{2+}$-GO/CNT papers. (d) N1s core-leveled XPS spectra of NG/CNT/$Co_3O_4$ paper.

Compared with the initial $Co^{2+}$-GO/CNT paper, there were 5.4 at. % of nitrogen in the NG/CNT/$Co_3O_4$ paper. The N1s core-leveled XPS spectra (Fig. 2d) indicated the presence of four types of nitrogen species, namely, pyrrolic N (400.1 eV), pyridinic N (399 eV), graphitic N (401 eV), pyridinic N-O (404 eV).[35, 36] Furthermore, the shifted C=C band of 284.2 eV to 284.9 eV in C1s core-leveled XPS spectra was attributed to the nitrogen doping in the NG/CNT/$Co_3O_4$ paper. Moreover, elemental mapping analysis further proved the homogeneous dispersions of C, N, O and Co elements in the composite paper (ESI, Fig. S3b-f†). These analyses well revealed the effective nitrogen doping in the paper by using the hydrothermal strategy. Interestingly, the content of the nitrogen doped in the composite paper was controllable by changing the concentration of the ammonia solution in the hydrothermal procedure. As shown from XPS spectra (ESI, Fig. S6†), the nitrogen content was increased from 4.8 to 8.2 at. % with correspondingly improving the ammonia concentration from 1.6 to 13.3 vol. %.

For comparison, the controlled samples of NG/$Co_3O_4$, and NG/CNT papers were fabricated by the similar preparation procedures to NG/CNT/$Co_3O_4$ paper, just without addition of CNT or cobalt precursor in the initial mixtures. Another controlled sample called physically-mixed NG/CNT/$Co_3O_4$ composite paper was prepared by the hydrothermal treatment of the assembled paper composed of GO, CNT and pre-synthesized $Co_3O_4$ nanoparticles in the ammonia solution, as proved by XRD pattern (ESI, Fig. S7†). Herein, NG/$Co_3O_4$ paper was selected as the example to make detailed characterizations. SEM images of the typical NG/$Co_3O_4$ paper showed an ordered multilayer structure of the thin NG sheets (ESI, Fig. S8a-c†). Abundant of $Co_3O_4$ nanoparticles

were observed both on the surface and inner of the NG layers. XRD pattern confirmed the formation of $Co_3O_4$ phase with a face-centered cubic structure (JCPDS No. 42-1467) in the paper (ESI, Fig. S8d†). The survey XPS spectrum showed that NG/$Co_3O_4$ paper was composed of C, N, O and Co elements (ESI, Fig. S9a†). The N percentage of the NG/$Co_3O_4$ paper was reached 7.2 at %, deconvoluted into four types of N species, as shown in the N1s core-leveled XPS spectra (ESI, Fig. S9b†). The weakened intensities of oxygen-containing carbon in the C1s core-leveled XPS spectra revealed the effective reduction of GO to graphene sheets (ESI, Fig. S9c†).

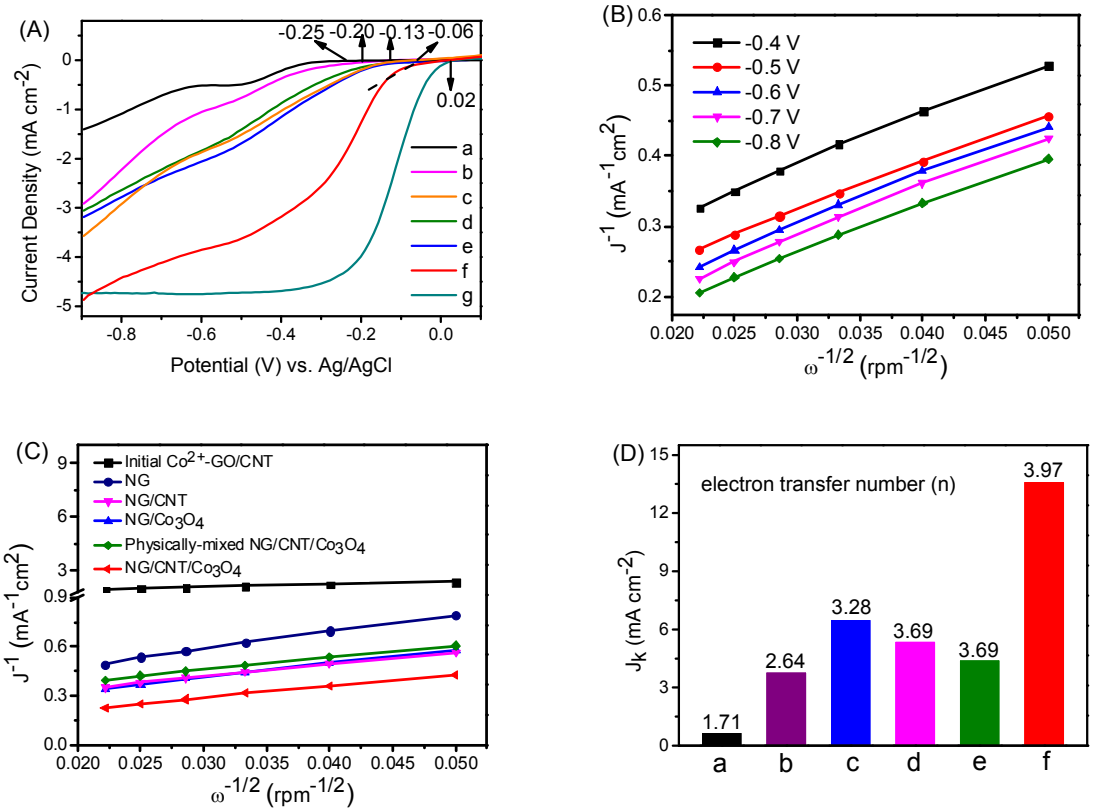


**Fig. 3** (A) RDE curves of samples (a-g) in $O_2$-saturated 0.1 M KOH solution with rotation speed of 1600 rpm and sweep rate of 10 mV $s^{-1}$. (B) K-L plots ($J^{-1}$ versus $\omega^{-1/2}$) of NG/CNT/$Co_3O_4$ paper at different potentials. (C) K-L plots of a series of prepared catalysts at -0.7 V. (D) Electrochemical activities given as the kinetic-limited current density ($J_k$) at -0.7 V for samples (a-f). Herein, a: initial $Co^{2+}$-GO/CNT; b: NG; c: NG/CNT; d: NG/$Co_3O_4$; e: physically-mixed NG/CNT/$Co_3O_4$; f: NG/CNT/$Co_3O_4$ paper; g: commercial Pt/C.

**ORR electrocatalytic performances of flexible papers**

Rotating-disk electrode (RDE) measurements were carried out to investigate the ORR activities of a series of samples in $O_2$-saturated 0.1 M KOH electrolyte at a scan rate of 10 mV $s^{-1}$, including initial $Co^{2+}$-GO/CNT, NG, NG/$Co_3O_4$, NG/CNT, physically-mixed NG/CNT/$Co_3O_4$, NG/CNT/$Co_3O_4$ papers and commercial 20 wt % Pt/C. As shown in RDE curves (**Fig. 3**A), the initial $Co^{2+}$-GO/CNT paper without hydrothermal treatment exhibited the lowest ORR electrocatalytic activity. Among these prepared freestanding catalysts, NG/CNT/$Co_3O_4$ paper showed the enhanced ORR performance with positive onset potential and large current density comparable to that of the commercial Pt/C. It was contributed to the synergistic effects of three components and the interpenetrated network structure in combinations of NG with CNT, effectively increasing the basal spacing and the electrical conductivity.[37] The physically-mixed NG/CNT/$Co_3O_4$ paper was inferior to the NG/CNT/$Co_3O_4$ paper in catalytic activity, suggesting that the high catalytic activity of NG/CNT/$Co_3O_4$ paper was attributed to the strong coupling between $Co_3O_4$ nanoparticles and NG or CNTs.[18] Furthermore, RDE curves of NG/CNT/$Co_3O_4$ paper at various rotation speeds were measured to reveal its ORR kinetic performance (ESI, Fig. S10†). The corresponding Koutecky-Levich (K-L) plots ($J^{-1}$ vs. $\omega^{-1/2}$) at various electrode potentials exhibited good linearity (Fig. 3B). The linearity and parallelism of the K-L plots usually suggested first-order reaction kinetics toward the concentration of dissolved oxygen and similar electron transfer numbers for ORR at different potentials.[38] The electron transfer number (n) was calculated to be 3.97 at -0.7 V from the slope of K-L plot,[2] indicating that NG/CNT/$Co_3O_4$ paper favored a $4e^-$ oxygen reduction process. Fig. 3C showed the K-L plots of a series of the controlled samples at -0.7 V according to their corresponding RDE curves (ESI, Fig. S11-S15†). The electron transfer number (n) and calculated kinetic-limited current density ($J_K$) value of different catalysts were clearly drawn

(Fig. 3D). Except for the $4e^-$ ORR process, NG/CNT/$Co_3O_4$ paper exhibited the $J_K$ value of 13.57 mA $cm^{-2}$ at -0.7 V, much higher than that of NG/CNT and NG/$Co_3O_4$ papers of 6.45 and 5.34 mA $cm^{-2}$, respectively.

A series of the NG/CNT/$Co_3O_4$ composite papers were prepared to study the influence of the relative component contents on the ORR electrocatalytic activity. SEM images clearly revealed the effect of the concentration of the cobalt ions on the size of the cobalt oxide nanoparticles, while keeping the constant weight ratio of CNT and GO to 1:10 (ESI, Fig. S16†). With improving the content of cobalt precursor from 0.1 to 0.2 mmol, the size of $Co_3O_4$ nanoparticles was grown from 15 to 25 nm. When increasing the used cobalt precursor to 0.3 mmol, the $Co_3O_4$ nanoparticles were aggregated to about 70 nm. The further increase of cobalt precursor led to the bigger $Co_3O_4$ nanoparticles, as investigated from the size range from 150 to 300 nm in SEM image (ESI, Fig. S16d†). RDE curves showed the changes of ORR activities with increasing the used cobalt nitrate precursor (ESI, Fig. S17a†). The catalyst exhibited the enhanced ORR activity with the proper contents of cobalt nitrate from 0 to 0.2 mmol, indicating that cobalt oxide species at the interface of NG or CNTs were served as the active reaction sites in the paper for ORR.[16] When further increasing cobalt nitrate, the corresponding ORR activities were weakened, probably due to the low activities of the over-growth of cobalt oxide species in the composite papers.[19] Furthermore, it was investigated that the relative content of CNT and GO had the important effect on the ORR performances of the composite paper (ESI, Fig. S17b†). The enhanced electrocatalytic activity of the NG/CNT/$Co_3O_4$ paper with the optimized weight ratio of CNT and GO of 1:10 indicated the benefit of the interpenetrated network between CNT and GO to ORR.

The NG/CNT/$Co_3O_4$ paper with different aging time in ammonia solution also affected the ORR

electrocatalytic activity. As shown in the RDE curves (ESI, Fig. S18a†), with prolonging the hydrothermal time from 0 to 2 h, the catalysts exhibited the remarkably enhanced ORR activity due to the time-dependent formation of $Co_3O_4$ nanoparticles and reduction of GO to NG in the NG/CNT/$Co_3O_4$ composite paper as revealed from the evolutions of XRD patterns (ESI, Fig. S1†). When further increasing the hydrothermal time, its corresponding ORR activity was slightly weakened, due to the low conductivity resulted from the over-growth of cobalt oxide species in the product. Moreover, RDE curves opened out the great influence of the thickness of the composite paper on its ORR performance (ESI, Fig. S18b†). It was revealed that too thick composite paper seriously weakened its electrocatalytic activity, due to the sluggish transport of the electrolytes and electrons in the catalyst.

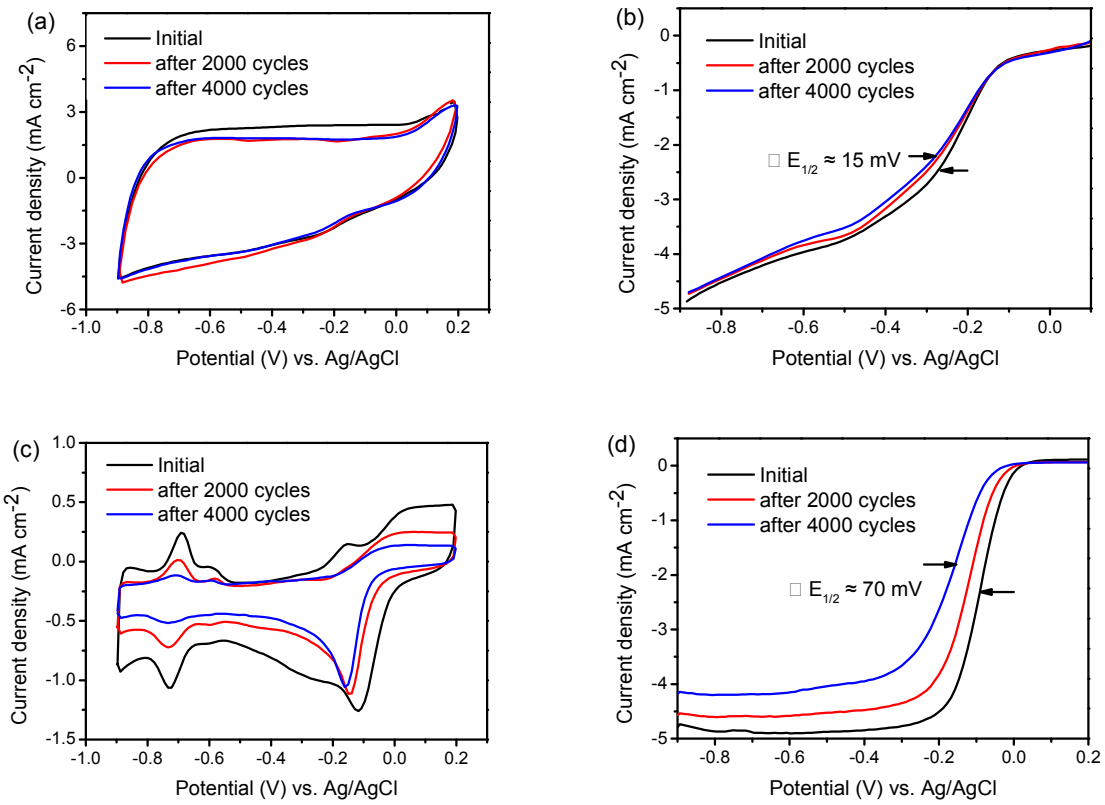


**Fig. 4** Cyclic voltammograms (a) and RDE voltammograms (b) of NG/CNT/$Co_3O_4$ paper with 4000 cycles in $O_2$-saturated 0.1 M KOH; Cyclic voltammograms (c) and RDE voltammograms (d) of

Pt/C with 4000 cycles in $O_2$-saturated 0.1 M KOH.

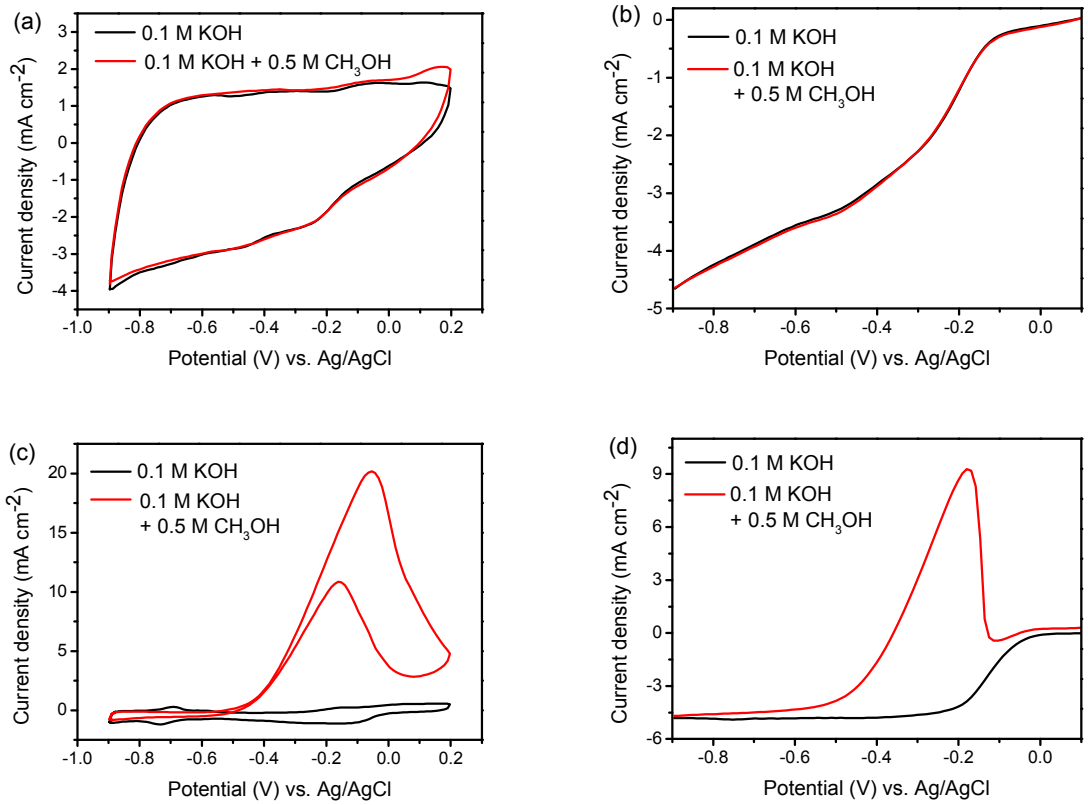


**Fig. 5** Cyclic voltammograms (a) and RDE voltammograms (b) of NG/CNT/$Co_3O_4$ in $O_2$-saturated 0.1 M KOH with or without 0.5 M methanol; Cyclic voltammograms (c) and RDE voltammograms (d) of Pt/C in $O_2$-saturated 0.1 M KOH with or without 0.5 M methanol.

**Cycling stability and methanol-tolerant capability of the electrocatalyst**

The long-term durability of the NG/CNT/$Co_3O_4$ paper was considered as another important factor to evaluate the ORR performance. No remarkable changes were found in the CV curves of NG/CNT/$Co_3O_4$ paper by performing continuous 4000 potential cycles between -0.9 and 0.2 V at 100 mV $s^{-1}$ in $O_2$-saturated 0.1 M KOH (**Fig. 4**a). Furthermore, the RDE curves of NG/CNT/$Co_3O_4$ catalyst (Fig. 4b) showed that after 4000 cycles, the half-wave potential $E_{1/2}$ exhibited a slightly negative shift of ~ 15 mV in $O_2$-saturated 0.1 M KOH. However, the serious attenuation was investigated from the 4000 cycles of CV and RDE curves of the commercial Pt/C catalyst, respectively (Fig. 4c and 4d). Moreover, the promising ORR catalysts exhibited the high catalytic

selectivity for cathode reaction against the oxidation of methanol due to the possible cross-over effect of methanol through the polymer electrolyte membrane from anode to cathode in direct methanol fuel cells.[39] To examine the tolerance of the catalyst to the methanol crossover effects, CV and RDE curves were measured in $O_2$-saturated 0.1 M KOH with and without addition of 0.5 M methanol, respectively. It was found that the NG/CNT/$Co_3O_4$ catalyst exhibited the strong ability to avoid methanol crossover effects (**Fig. 5**a and 5b). In contrast, there was an obvious decrease in the ORR activity of Pt/C due to the competitive reaction between oxygen reduction and methanol oxidation (Fig. 5c and 5d).[40,41]

**Conclusions**

In summary, a new kind of flexible NG/CNT/$Co_3O_4$ composite paper has been developed by a convenient but effective strategy in which combines the scaled-up self-assembly process with the following hydrothermal treatment. Doping of nitrogen, reduction of GO and *in-situ* formation of $Co_3O_4$ nanoparticles in the freestanding paper simultaneously occur in the hydrothermal process in the ammonia solution. NG/CNT/$Co_3O_4$ paper exhibits the remarkably enhanced ORR electrocatalytic activities due to the synergistic effects of three components and the spacing effect of CNTs between the graphene nanosheets. Furthermore, the obtained paper shows the better durability and tolerance to methanol poisoning effects than the commercial Pt/C catalyst. The present work provides a feasible way for the design and large-scale synthesis of freestanding electrocatalyst with high activity for ORR under the mild condition, which can be further extended to produce hybrid materials with broad applications in electronics, supercapacitors and lithium ion batteries.

**Acknowledgements**

We acknowledge the funding support from the Ministry of Science and Technology of China (Grant 2012BAD32B05-4), the National Basic Research Program of China (Grants 2010CB934700, 2013CB933900, 2014CB931800), the National Natural Science Foundation of China (Grants 91022032, 91227103, 21061160492), and the Chinese Academy of Sciences (Grant KJZD-EW-M01-1). H. P. C. thanks the Program for New Century Excellent Talents in University the Fundamental Research Funds for the Central Universities (2013JYXR0654), Hefei Institutes of Physics Science, CAS (Grant 2012FXCX008), China Postdoctoral Science Foundation (Grant 20110490086), and the Foundation for the Author of Excellent Doctoral Dissertation of CAS.

**Notes and references**

1 B. C. Steele and A. Heinzel, *Nature,* 2001, **414**, 345-352.

2 L. Qu, Y. Liu, J.-B. Baek and L. Dai, *ACS Nano,* 2010, **4**, 1321-1326.

3 M.-R. Gao, Y.-F. Xu, J. Jiang and S.-H. Yu, *Chem. Soc. Rev.,* 2013, **42**, 2986-3017.

4 J. Xu, P. Gao and T. Zhao, *Energy Environ. Sci.,* 2012, **5**, 5333-5339.

5 A. Ishihara, Y. Ohgi, K. Matsuzawa, S. Mitsushima and K.-I. Ota, *Electrochim. Acta,* 2010, **55**, 8005-8012.

6 G. Wu, K. L. More, C. M. Johnston and P. Zelenay, *Science,* 2011, **332**, 443-447.

7 R. Bashyam and P. Zelenay, *Nature,* 2006, **443**, 63-66.

8 Y. Zheng, Y. Jiao, M. Jaroniec, Y. Jin and S. Z. Qiao, *Small,* 2012, **8**, 3550-3566.

9 H. Wang, T. Maiyalagan and X. Wang, *Acs Catalysis,* 2012, **2**, 781-794.

10 K. Gong, F. Du, Z. Xia, M. Durstock and L. Dai, *Science,* 2009, **323**, 760-764.

11 K. Parvez, S. Yang, Y. Hernandez, A. Winter, A. Turchanin, X. Feng and K. Müllen, *ACS Nano,* 2012, **6**, 9541-9550.

12 C. Wang, Y. Zhou, L. He, T.-W. Ng, G. Hong, Q.-H. Wu, F. Gao, C.-S. Lee and W. Zhang, *Nanoscale,* 2013, **5**, 600-605.

13 L. Panchakarla, K. Subrahmanyam, S. Saha, A. Govindaraj, H. Krishnamurthy, U. Waghmare

and C. Rao, *Adv. Mater.,* 2009, **21**, 4726-4730.

14 D. Yu, Q. Zhang and L. Dai, *J. Am. Chem. Soc.,* 2010, **132**, 15127-15129.

15 Y. Zheng, Y. Jiao, L. Ge, M. Jaroniec and S. Z. Qiao, *Angew. Chem. Int. Ed.,* 2013, **125**, 3192-3198.

16 Y. Liang, Y. Li, H. Wang, J. Zhou, J. Wang, T. Regier and H. Dai, *Nat. Mater.,* 2011, **10**, 780-786.

17 Y. Liang, H. Wang, P. Diao, W. Chang, G. Hong, Y. Li, M. Gong, L. Xie, J. Zhou and J. Wang, *J. Am. Chem. Soc.,* 2012, **134**, 15849-15857.

18 Y. Liang, H. Wang, J. Zhou, Y. Li, J. Wang, T. Regier and H. Dai, *J. Am. Chem. Soc.,* 2012, **134**, 3517-3523.

19 Z.-S. Wu, S. Yang, Y. Sun, K. Parvez, X. Feng and K. Müllen, *J. Am. Chem. Soc.,* 2012, **134**, 9082-9085.

20 G. Zhang, B. Y. Xia, X. Wang and X. W. Lou, *Adv. Mater.,* 2014, **26**, 2408-2412.

21 H. Wang, Y. Liang, Y. Li and H. Dai, *Angew. Chem. Int. Ed.,* 2011, **50**, 10969-10972.

22 P. Chen, T.-Y. Xiao, H.-H. Li, J.-J. Yang, Z. Wang, H.-B. Yao and S.-H. Yu, *ACS Nano,* 2011, **6**, 712-719.

23 B. Xia, Y. Yan, X. Wang and X. W. Lou, *Mater. Horiz.,* 2014, DOI: 10.1039/C1034MH00040D.

24 V. C. Tung, L.-M. Chen, M. J. Allen, J. K. Wassei, K. Nelson, R. B. Kaner and Y. Yang, *Nano Lett.,* 2009, **9**, 1949-1955.

25 L. L. Zhang, Z. Xiong and X. Zhao, *ACS Nano,* 2010, **4**, 7030-7036.

26 E. Yoo, J. Kim, E. Hosono, H.-S. Zhou, T. Kudo and I. Honma, *Nano Lett.,* 2008, **8**, 2277-2282.

27 C. Yuan, L. Yang, L. Hou, J. Li, Y. Sun, X. Zhang, L. Shen, X. Lu, S. Xiong and X. W. Lou, *Adv. Funct. Mater.,* 2012, **22**, 2560-2566.

28 P. Chen, T. Y. Xiao, Y. H. Qian, S. S. Li and S. H. Yu, *Adv. Mater.,* 2013, **25**, 3192-3196.

29 Q. Su, Y. Liang, X. Feng and K. Müllen, *Chem. Comm.,* 2010, **46**, 8279-8281.

30 H.-P. Cong, X.-C. Ren, P. Wang and S.-H. Yu, *Energ Environ. Sci.,* 2013, **6**, 1185-1191.

31 W. S. Hummers and R. E. Offeman, *J. Am. Chem. Soc.,* 1958, **80**, 1339-1339.

32 D. Cai, M. Song and C. Xu, *Adv. Mater. ,* 2008, **20**, 1706-1709.

33 Z.-S. Wu, W. Ren, L. Wen, L. Gao, J. Zhao, Z. Chen, G. Zhou, F. Li and H.-M. Cheng, *ACS Nano,* 2010, **4**, 3187-3194.

34 Z.-H. Sheng, L. Shao, J.-J. Chen, W.-J. Bao, F.-B. Wang and X.-H. Xia, *ACS Nano,* 2011, **5**, 4350-4358.

35 J. Casanovas, J. M. Ricart, J. Rubio, F. Illas and J. M. Jiménez-Mateos, *J. Am. Chem. Soc.,* 1996, **118**, 8071-8076.

36 P. H. Matter, L. Zhang and U. S. Ozkan, *J. Catal.,* 2006, **239**, 83-96.

37 Z. Fan, J. Yan, L. Zhi, Q. Zhang, T. Wei, J. Feng, M. Zhang, W. Qian and F. Wei, *Adv. Mater.,* 2010, **22**, 3723-3728.

38 K. Mayrhofer, D. Strmcnik, B. B. Blizanac, V. Stamenkovic, M. Arenz and N. M. Markovic, *Electrochim. Acta,* 2008, **53**, 3181-3188.

39 A. Arico, S. Srinivasan and V. Antonucci, *Fuel cells,* 2001, **1**, 133-161.

40 H. Yang, N. Alonso-Vante, J.-M. Léger and C. Lamy, *J. Phys. Chem. B,* 2004, **108**, 1938-1947.

41 Y. Li, W. Zhou, H. Wang, L. Xie, Y. Liang, F. Wei, J.-C. Idrobo, S. J. Pennycook and H. Dai, *Nat. Nanotechnol.,* 2012, **7**, 394-400.